Forward Λ production and nuclear stopping power in d+Au collisions at $\sqrt{s_{NN}} = 200$ GeV

B. I. Abelev,[9] M. M. Aggarwal,[30] Z. Ahammed,[45] B. D. Anderson,[20] D. Arkhipkin,[13] G. S. Averichev,[12] Y. Bai,[28] J. Balewski,[17] O. Barannikova,[9] L. S. Barnby,[2] J. Baudot,[18] S. Baumgart,[50] V. V. Belaga,[12] A. Bellingeri-Laurikainen,[40] R. Bellwied,[48] F. Benedosso,[28] R. R. Betts,[9] S. Bhardwaj,[35] A. Bhasin,[19] A. K. Bhati,[30] H. Bichsel,[47] J. Bielcik,[50] J. Bielcikova,[50] L. C. Bland,[3] S.-L. Blyth,[22] M. Bombara,[2] B. E. Bonner,[36] M. Botje,[28] J. Bouchet,[40] A. V. Brandin,[26] A. Bravar,[3] T. P. Burton,[2] M. Bystersky,[11] X. Z. Cai,[39] H. Caines,[50] M. Calderón de la Barca Sánchez,[6] J. Callner,[9] O. Catu,[50] D. Cebra,[6] M. C. Cervantes,[41] Z. Chajecki,[29] P. Chaloupka,[11] S. Chattopadhyay,[45] H. F. Chen,[38] J. H. Chen,[39] J. Y. Chen,[49] J. Cheng,[43] M. Cherney,[10] A. Chikanian,[50] W. Christie,[3] S. U. Chung,[3] R. F. Clarke,[41] M. J. M. Codrington,[41] J. P. Coffin,[18] T. M. Cormier,[48] M. R. Cosentino,[37] J. G. Cramer,[47] H. J. Crawford,[5] D. Das,[45] S. Dash,[15] M. Daugherity,[42] M. M. de Moura,[37] T. G. Dedovich,[12] M. DePhillips,[3] A. A. Derevschikov,[32] L. Didenko,[3] T. Dietel,[14] P. Djawotho,[17] S. M. Dogra,[19] X. Dong,[22] J. L. Drachenberg,[41] J. E. Draper,[6] F. Du,[50] V. B. Dunin,[12] J. C. Dunlop,[3] M. R. Dutta Mazumdar,[45] V. Eckardt,[24] W. R. Edwards,[22] L. G. Efimov,[12] V. Emelianov,[26] J. Engelage,[5] G. Eppley,[36] B. Erazmus,[40] M. Estienne,[18] P. Fachini,[3] R. Fatemi,[23] J. Fedorisin,[12] A. Feng,[49] P. Filip,[13] E. Finch,[50] V. Fine,[3] Y. Fisyak,[3] J. Fu,[49] C. A. Gagliardi,[41] L. Gaillard,[2] M. S. Ganti,[45] E. Garcia-Solis,[9] V. Ghazikhanian,[7] P. Ghosh,[45] Y. N. Gorbunov,[10] H. Gos,[46] O. Grebenyuk,[28] D. Grosnick,[44] B. Grube,[34] S. M. Guertin,[7] K. S. F. F. Guimaraes,[37] N. Gupta,[19] B. Haag,[6] T. J. Hallman,[3] A. Hamed,[41] J. W. Harris,[50] W. He,[17] M. Heinz,[50] T. W. Henry,[41] S. Heppelmann,[31] B. Hippolyte,[18] A. Hirsch,[33] E. Hjort,[22] A. M. Hoffman,[23] G. W. Hoffmann,[42] D. J. Hofman,[9] R. S. Hollis,[9] M. J. Horner,[22] H. Z. Huang,[7] E. W. Hughes,[4] T. J. Humanic,[29] G. Igo,[7] A. Iordanova,[9] P. Jacobs,[22] W. W. Jacobs,[17] P. Jakl,[11] F. Jia,[21] P. G. Jones,[2] E. G. Judd,[5] S. Kabana,[40] K. Kang,[43] J. Kapitan,[11] M. Kaplan,[8] D. Keane,[20] A. Kechechyan,[12] D. Kettler,[47] V. Yu. Khodyrev,[32] J. Kiryluk,[22] A. Kisiel,[29] E. M. Kislov,[12] S. R. Klein,[22] A. G. Knospe,[50] A. Kocoloski,[23] D. D. Koetke,[44] T. Kollegger,[14] M. Kopytine,[20] L. Kotchenda,[26] V. Kouchpil,[11] K. L. Kowalik,[22] P. Kravtsov,[26] V. I. Kravtsov,[32] K. Krueger,[1] C. Kuhn,[18] A. I. Kulikov,[12] A. Kumar,[30] P. Kurnadi,[7] A. A. Kuznetsov,[12] M. A. C. Lamont,[50] J. M. Landgraf,[3] S. Lange,[14] S. LaPointe,[48] F. Laue,[3] J. Lauret,[3] A. Lebedev,[3] R. Lednicky,[13] C.-H. Lee,[34] S. Lehocka,[12] M. J. LeVine,[3] C. Li,[38] Q. Li,[48] Y. Li,[43] G. Lin,[50] X. Lin,[49] S. J. Lindenbaum,[27] M. A. Lisa,[29] F. Liu,[49] H. Liu,[38] J. Liu,[36] L. Liu,[49] T. Ljubicic,[3] W. J. Llope,[36] R. S. Longacre,[3] W. A. Love,[3] Y. Lu,[49] T. Ludlam,[3] D. Lynn,[3] G. L. Ma,[39] J. G. Ma,[7] Y. G. Ma,[39] D. P. Mahapatra,[15] R. Majka,[50] L. K. Mangotra,[19] R. Manweiler,[44] S. Margetis,[20] C. Markert,[42] L. Martin,[40] H. S. Matis,[22] Yu. A. Matulenko,[32] C. J. McClain,[1] T. S. McShane,[10] Yu. Melnick,[32] A. Meschanin,[32] J. Millane,[23] M. L. Miller,[23] N. G. Minaev,[32] S. Mioduszewski,[41] A. Mischke,[28] J. Mitchell,[36] B. Mohanty,[22] D. A. Morozov,[32] M. G. Munhoz,[37] B. K. Nandi,[16] C. Nattrass,[50] T. K. Nayak,[45] J. M. Nelson,[2] C. Nepali,[20] P. K. Netrakanti,[33] L. V. Nogach,[32] S. B. Nurushev,[32] G. Odyniec,[22] A. Ogawa,[3] V. Okorokov,[26] M. Oldenburg,[22] D. Olson,[22] M. Pachr,[11] S. K. Pal,[45] Y. Panebratsev,[12] A. I. Pavlinov,[48] T. Pawlak,[46] T. Peitzmann,[28] V. Perevoztchikov,[3] C. Perkins,[5] W. Peryt,[46] S. C. Phatak,[15] M. Planinic,[51] J. Pluta,[46] N. Poljak,[51] N. Porile,[33] A. M. Poskanzer,[22] M. Potekhin,[3] E. Potrebenikova,[12] B. V. K. S. Potukuchi,[19] D. Prindle,[47] C. Pruneau,[48] N. K. Pruthi,[30] J. Putschke,[22] I. A. Qattan,[17] R. Raniwala,[35] S. Raniwala,[35] R. L. Ray,[42] D. Relyea,[4] A. Ridiger,[26] H. G. Ritter,[22] J. B. Roberts,[36] O. V. Rogachevskiy,[12] J. L. Romero,[6] A. Rose,[22] C. Roy,[40] L. Ruan,[22] M. J. Russcher,[28] R. Sahoo,[15] I. Sakrejda,[22] T. Sakuma,[23] S. Salur,[50] J. Sandweiss,[50] M. Sarsour,[41] P. S. Sazhin,[12] J. Schambach,[42] R. P. Scharenberg,[33] N. Schmitz,[24] J. Seger,[10] I. Selyuzhenkov,[48] P. Seyboth,[24] A. Shabetai,[18] E. Shahaliev,[12] M. Shao,[38] M. Sharma,[30] W. Q. Shen,[39] S. S. Shimanskiy,[12] E. P. Sichtermann,[22] F. Simon,[23] R. N. Singaraju,[45] N. Smirnov,[50] R. Snellings,[28] P. Sorensen,[3] J. Sowinski,[17] J. Speltz,[18] H. M. Spinka,[1] B. Srivastava,[33] A. Stadnik,[12] T. D. S. Stanislaus,[44] D. Staszak,[7] R. Stock,[14] M. Strikhanov,[26] B. Stringfellow,[33] A. A. P. Suaide,[37] M. C. Suarez,[9] N. L. Subba,[20] M. Sumbera,[11] X. M. Sun,[22] Z. Sun,[21] B. Surrow,[23] T. J. M. Symons,[22] A. Szanto de Toledo,[37] J. Takahashi,[37] A. H. Tang,[3] T. Tarnowsky,[33] J. H. Thomas,[22] A. R. Timmins,[2] S. Timoshenko,[26] M. Tokarev,[12] T. A. Trainor,[47] S. Trentalange,[7] R. E. Tribble,[41] O. D. Tsai,[7] J. Ulery,[33] T. Ullrich,[3] D. G. Underwood,[1] G. Van Buren,[3] N. van der Kolk,[28] M. van Leeuwen,[22] A. M. Vander Molen,[25] R. Varma,[16] I. M. Vasilevski,[13] A. N. Vasiliev,[32] R. Vernet,[18] S. E. Vigdor,[17] Y. P. Viyogi,[15] S. Vokal,[12] S. A. Voloshin,[48] M. Wada,[10] W. T. Waggoner,[10] F. Wang,[33] G. Wang,[7] J. S. Wang,[21] X. L. Wang,[38] Y. Wang,[43] J. C. Webb,[44] G. D. Westfall,[25] C. Whitten Jr.,[7] H. Wieman,[22] S. W. Wissink,[17] R. Witt,[50] J. Wu,[38] Y. Wu,[49] N. Xu,[22] Q. H. Xu,[22] Z. Xu,[3] P. Yepes,[36] I-K. Yoo,[34] Q. Yue,[43] V. I. Yurevich,[12] M. Zawisza,[46] W. Zhan,[21] H. Zhang,[3] W. M. Zhang,[20] Y. Zhang,[38] Z. P. Zhang,[38] Y. Zhao,[38] C. Zhong,[39] J. Zhou,[36] R. Zoulkarneev,[13] Y. Zoulkarneeva,[13] A. N. Zubarev,[12] and J. X. Zuo[39]

(STAR Collaboration)

[1]*Argonne National Laboratory, Argonne, Illinois 60439, USA*
[2]*University of Birmingham, Birmingham, United Kingdom*
[3]*Brookhaven National Laboratory, Upton, New York 11973, USA*
[4]*California Institute of Technology, Pasadena, California 91125, USA*
[5]*University of California, Berkeley, California 94720, USA*
[6]*University of California, Davis, California 95616, USA*
[7]*University of California, Los Angeles, California 90095, USA*
[8]*Carnegie Mellon University, Pittsburgh, Pennsylvania 15213, USA*
[9]*University of Illinois at Chicago, Chicago, Illinois 60607, USA*
[10]*Creighton University, Omaha, Nebraska 68178, USA*

 ©2007 The American Physical Society

[11]*Nuclear Physics Institute AS CR, 250 68 Řež/Prague, Czech Republic*
[12]*Laboratory for High Energy (JINR), Dubna, Russia*
[13]*Particle Physics Laboratory (JINR), Dubna, Russia*
[14]*University of Frankfurt, Frankfurt, Germany*
[15]*Institute of Physics, Bhubaneswar 751005, India*
[16]*Indian Institute of Technology, Mumbai, India*
[17]*Indiana University, Bloomington, Indiana 47408, USA*
[18]*Institut de Recherches Subatomiques, Strasbourg, France*
[19]*University of Jammu, Jammu 180001, India*
[20]*Kent State University, Kent, Ohio 44242, USA*
[21]*Institute of Modern Physics, Lanzhou, People's Republic of China*
[22]*Lawrence Berkeley National Laboratory, Berkeley, California 94720, USA*
[23]*Massachusetts Institute of Technology, Cambridge, MA 02139-4307, USA*
[24]*Max-Planck-Institut für Physik, Munich, Germany*
[25]*Michigan State University, East Lansing, Michigan 48824, USA*
[26]*Moscow Engineering Physics Institute, Moscow, Russia*
[27]*City College of New York, New York City, New York 10031, USA*
[28]*NIKHEF and Utrecht University, Amsterdam, The Netherlands*
[29]*Ohio State University, Columbus, Ohio 43210, USA*
[30]*Panjab University, Chandigarh 160014, India*
[31]*Pennsylvania State University, University Park, Pennsylvania 16802, USA*
[32]*Institute of High Energy Physics, Protvino, Russia*
[33]*Purdue University, West Lafayette, Indiana 47907, USA*
[34]*Pusan National University, Pusan, Republic of Korea*
[35]*University of Rajasthan, Jaipur 302004, India*
[36]*Rice University, Houston, Texas 77251, USA*
[37]*Universidade de Sao Paulo, Sao Paulo, Brazil*
[38]*University of Science & Technology of China, Hefei 230026, People's Republic of China*
[39]*Shanghai Institute of Applied Physics, Shanghai 201800, People's Republic of China*
[40]*SUBATECH, Nantes, France*
[41]*Texas A&M University, College Station, Texas 77843, USA*
[42]*University of Texas, Austin, Texas 78712, USA*
[43]*Tsinghua University, Beijing 100084, People's Republic of China*
[44]*Valparaiso University, Valparaiso, Indiana 46383, USA*
[45]*Variable Energy Cyclotron Centre, Kolkata 700064, India*
[46]*Warsaw University of Technology, Warsaw, Poland*
[47]*University of Washington, Seattle, Washington 98195, USA*
[48]*Wayne State University, Detroit, Michigan 48201, USA*
[49]*Institute of Particle Physics, CCNU (HZNU), Wuhan 430079, People's Republic of China*
[50]*Yale University, New Haven, Connecticut 06520, USA*
[51]*University of Zagreb, Zagreb, HR-10002, Croatia*
(Received 4 June 2007; published 18 December 2007)

We report the measurement of Λ and $\bar{\Lambda}$ yields and inverse slope parameters in d+Au collisions at $\sqrt{s_{NN}} =$ 200 GeV at forward and backward rapidities ($y = \pm 2.75$), using data from the STAR forward time projection chambers. The contributions of different processes to baryon transport and particle production are probed exploiting the inherent asymmetry of the d+Au system. Comparisons to model calculations show that baryon transport on the deuteron side is consistent with multiple collisions of the deuteron nucleons with gold participants. On the gold side, HIJING-based models without a hadronic rescattering phase do not describe the measured particle yields, while models that include target remnants or hadronic rescattering do. The multichain model can provide a good description of the net baryon density in d+Au collisions at energies currently available at the BNL Relativistic Heavy Ion Collider, and the derived parameters of the model agree with those from nuclear collisions at lower energies.

DOI: 10.1103/PhysRevC.76.064904 PACS number(s): 25.75.Dw

I. INTRODUCTION

The production of strange baryons has been studied extensively in heavy-ion collisions at the BNL Relativistic Heavy Ion Collider (RHIC) [1]. So far, these measurements have been concentrated around midrapidity. In d+Au collisions, the study of particle production away from midrapidity is

especially appealing, since the inherent asymmetry of these events allows the probing of different processes for particle production on the deuteron side (the side in the d beam direction, positive rapidity) and on the gold side (the side in the Au beam direction, negative rapidity) of the reaction. The deuteron side of the collision is expected to be dominated by multiple collisions of the incoming deuteron nucleons with gold participants and corresponding nuclear effects; while on the gold side, final state rescattering and soft processes in the nuclear breakup might contribute significantly. By studying the particle yields and the inverse slope parameters of Λ and $\bar{\Lambda}$ as a function of centrality, these effects are investigated. The centrality dependence of the yields can help illuminate the role of nuclear effects in the observed strangeness enhancement in Au+Au collisions [2,3].

In addition to providing information about strange particle production in asymmetric collisions, Λ and $\bar{\Lambda}$ production at forward rapidities in d+Au collisions also probes baryon transport and nuclear stopping power. The study of nuclear stopping power is a fundamental issue in heavy-ion physics [4], since this quantity is related to the amount of energy and baryon number that get transferred from the beam particles into the reaction zone. This influences the properties of possible new states of matter created in these collisions. For these studies, measurements at forward rapidities are crucial, since incomplete stopping is expected at collider energies [5]. This should lead to significant net baryon densities near beam rapidity; while at lower energies, the bulk of the net baryons are concentrated near midrapidity. At energies available at the CERN Super Proton Synchrotron (SPS), comprehensive studies of the rapidity distribution of net baryons in asymmetric collision systems demonstrate that the rapidity loss in these collisions depends mainly on the thickness of the nuclear target [6]. Recent theoretical work suggests that nuclear stopping may arise from gluon bremsstrahlung in cold nuclear matter [7]. A measurement of the mean rapidity loss of baryons in central Au+Au collisions at $\sqrt{s_{NN}} = 200$ GeV [8] and the comparison to such measurements in central Pb+Pb collisions at the SPS [9] indicate that a saturation of stopping is reached in central nucleus-nucleus reactions with respect to the center-of-mass energy at the top RHIC energy [8]. This is shown by the deviation from a linear scaling of the rapidity loss with collision energy observed at RHIC energies.

This paper presents the measurement of Λ and $\bar{\Lambda}$ particle yields and inverse slope parameters at forward ($y = 2.75 \pm 0.25$) and backward rapidity ($y = -2.75 \pm 0.25$) in d+Au collisions at $\sqrt{s_{NN}} = 200$ GeV. By comparing the particle yields to model calculations performed with the AMPT [10,11], EPOS [12], HIJING [13], and HIJING/B$\bar{\text{B}}$ [14,15] codes, information about the mechanisms for particle production in asymmetric collisions is gained. The net Λ yield $[dN/dy(\Lambda) - dN/dy(\bar{\Lambda})]$ as a function of centrality is compared with calculations based on the multichain model (MCM) [16], which was previously successfully applied to lower energy data. This comparison indicates that the baryon rapidity loss in d+Au collisions at RHIC is consistent with the predictions of the multichain model.

II. EXPERIMENTAL SETUP AND ANALYSIS TECHNIQUE

The data discussed here were taken with the solenoidal tracker (STAR) detector [17] at the RHIC accelerator facility. The minimum bias trigger used for the data in this analysis required at least one beam momentum neutron in the zero degree calorimeter (ZDC) in the Au beam direction. This trigger accepts $95 \pm 3\%$ of the d+Au hadronic cross section [18]. The main detectors for the present analysis were the two radial-drift forward time projection chambers (FTPCs) [19] that cover $2.5 < |\eta| < 4.0$ in pseudorapidity on both sides of the interaction region. The detector that sits on the side of the interaction region toward which the gold particles fly, and thus intercepts gold fragments, is referred to as FTPC-Au (negative rapidity). The detector on the deuteron side of the experiment is referred to as FTPC-d (positive rapidity). Data from the main TPC [20] of STAR is used to determine the event vertex and to provide a measure of the collision centrality, based on the charged particle multiplicity at midrapidity. This method of collision centrality determination avoids autocorrelations in the analysis, since different detectors are used for the measurements discussed here and for the centrality definition. The minimum bias data set is thus divided into three centrality bins, as suggested in Ref. [21]. The peripheral bin contains the 40–100% most peripheral events, the midcentral bin contains 20–40%, and the central bin contains the 20% most central events, as defined by the charged particle multiplicity. The number of binary collisions, the number of d, and the number of Au participants for each of these bins are determined using Monte Carlo Glauber calculations incorporating the Hulthén wave function of the deuteron [22]. Table I summarizes the Glauber calculation results. Contrary to the case of collisions of large, equal-sized nuclei, in d+Au collisions the mean number of binary collisions is smaller than the mean number of participants, since in most cases each Au nucleon only participates in one collision.

After event selection cuts, which required a reconstructed primary event vertex along the beam axis within 50 cm of the center of the detector system, 10^7 minimum bias events were accepted in the data sample. The vertex reconstruction efficiency was determined to be $93 \pm 1\%$ [18]. Since the vertex

TABLE I. Mean number of participants and mean number of binary collisions for minimum bias events and the three centrality classes, determined by Glauber calculations. Also given are the mean number of participants separated for the deuteron and the gold nucleus.

Centrality	$\langle N_{\text{part}} \rangle$	$\langle N_{\text{bin}} \rangle$
Minimum bias	8.3 ± 0.4	7.5 ± 0.4
Central (top 20%)	$15.7^{+1.2}_{-1.0}$	$15.0^{+1.3}_{-0.9}$
Midcentral (20–40%)	$11.2^{+1.1}_{-1.0}$	$10.6^{+0.8}_{-1.1}$
Peripheral (40–100%)	5.1 ± 0.4	4.2 ± 0.4
Centrality	$\langle N_{\text{part},d} \rangle$	$\langle N_{\text{part,Au}} \rangle$
Minimum bias	1.6	6.7
Central (top 20%)	2.0	13.7
Midcentral (20–40%)	1.9	9.3
Peripheral (40–100%)	1.4	3.7

reconstruction efficiency is a strong function of the number of tracks at midrapidity, only peripheral events are affected by not reconstructed vertices. All particle spectra and yields are corrected for trigger and vertex finding efficiencies.

The momentum resolution of the FTPCs was determined from simulations to be between about 10% and 20% for single charged tracks in the momentum and rapidity range covered by the present analysis. The momentum resolution for reconstructed Λ and $\bar{\Lambda}$ is on the order of 20%. The binning in p_T for the Λ and $\bar{\Lambda}$ spectra presented here is chosen accordingly.

In the FTPCs, Λ and $\bar{\Lambda}$ are reconstructed using their dominant decay modes $\Lambda \to p\pi^-$ and $\bar{\Lambda} \to \bar{p}\pi^+$, which have a branching ratio of 64%. Λ candidates are identified via displaced vertices. The FTPCs measure a maximum of ten points on a track. Because of the high momentum of particles in the forward rapidity region and consequently very similar energy loss dE/dx of different particle species in the detector gas, particle identification via the specific energy loss is impossible for singly charged hadrons. Thus, Λ candidates are formed from all pairs of one positive and one negative track which make up a possible decay vertex that is well separated from the main event vertex. These Λ candidates are conventionally referred to as V0 because of their topology and charge. In the present analysis, a minimum separation of 20 cm is required. This large minimum decay length leads to a reduction in the overall reconstruction efficiency, which is corrected for in the analysis.

In the case of Λ, the positive track is assumed to be a p, while the negative track is assumed to be a π^-. For $\bar{\Lambda}$, the positive track is assumed to be a π^+, while the negative track is assumed to be a $\bar{p}$. Since the most abundantly produced particle species are pions, this lack of particle identification introduces a considerable combinatoric background to the measurement. Strict cuts on the geometry of the assumed daughter tracks and the resulting Λ candidate efficiently reduce this background. The cut with the highest discriminating power was on the distance of closest approach (dca) of the decay daughters to the primary vertex, which should be relatively small for the p candidate and large for the π candidate, since the heavier decay daughter typically carries most of the momentum of the original particle and thus points back to the primary vertex, while the lighter daughter does not. This cut selects track pairs originating from a decay vertex well separated from the primary vertex and in addition reduces the background from $K_s^0 \to \pi^+\pi^-$ by favoring asymmetric decays. Additional cuts with high discriminating power were on the dca of the resulting Λ candidate and on the distance of the daughter tracks to the reconstructed decay vertex.

The remaining combinatoric background is determined by rotating the positive tracks by 180° with respect to the negative tracks in an event and then forming Λ candidates using the same cuts as on real data. With this method, the original spatial correlation of tracks is destroyed, removing real Λ and $\bar{\Lambda}$ from the sample. The combinatoric background, due to random track pairs that fulfill all analysis cuts, remains, since this depends on the track multiplicity and dca distributions which are preserved in the rotated sample. The subtraction of this background results in a 15–20% correction. A mechanism leading to the loss of Λ and $\bar{\Lambda}$ signals is a possible misidentification of the charge of one of the two decay daughters. The probability increases with the particle momentum, so it is much more likely for the proton candidate than for the pion candidate. This effect manifests itself in like-sign track pairs that fulfill the geometrical requirements for the Λ reconstruction. The size of this effect is determined with these like-sign pairs and is corrected for in the analysis. It is comparable in size to the remaining combinatoric background.

The major source of background remaining after these cuts and corrections is from $K_s^0 \to \pi^+\pi^-$, where one of the two daughter pions is assumed to be a proton. For the current analysis, a full GEANT detector simulation with a HIJING [13] generated K_s^0 distribution, where both the transverse momentum and the rapidity spectra of the particles were taken from the event generator, was used to model this background. On the deuteron side, it was verified that the K_s^0 yield taken from HIJING is in good agreement with d+Au data in the kinematic region covered by the FTPCs. This was done using the same analysis procedure as for Λ and $\bar{\Lambda}$, however, using different cuts to allow for the different kinematics of the K_s^0 decay.

For all V0s that pass the cuts, parameters such as the rapidity y, transverse momentum p_T, and invariant mass are calculated. In the present analysis, a rapidity range of $2.5 < |y| < 3.0$ was chosen, since this range is fully within the FTPC acceptance over the transverse momentum range of $0.5 < p_T < 2.0$ GeV/c used in the analysis.

Figure 1(a) shows the invariant mass distribution for Λ candidates on the deuteron side in the p_T range 0.5–2.0 GeV/c for d+Au minimum bias events. Also shown is the background contribution due to K_s^0 decays estimated from HIJING events. This background is subtracted, resulting in the Λ and $\bar{\Lambda}$ invariant mass distributions shown for the deuteron side in Fig. 1(b) and for the gold side in Fig. 1(c). On the gold side, the p_T range is restricted to 0.7–2.0 GeV/c, as discussed later in Sec. III. From Gaussian fits to the central part of the invariant mass distributions, a mass of 1.116 GeV/c^2 was determined for both Λ and $\bar{\Lambda}$ on both sides of the collision, in good agreement with the literature value. The width of the mass peak, given by the σ of the fit, is 24 MeV/c^2 for the deuteron side and 26 MeV/c^2 for the gold side, driven entirely by the detector resolution. The reconstructed mass is independent of centrality, but shows a slight p_T dependence due to the p_T dependent detector resolution. The variation over the studied transverse momentum range is around 10 MeV/c^2, with lower values at low p_T and higher values at high p_T. The observed invariant mass distributions are reproduced by a full GEANT simulation taking into account the detector response.

The raw particle yields are extracted by summing up the bin contents of the background-subtracted invariant mass distributions from 1.08 to 1.24 GeV/c^2. To get from the raw particle yields to corrected yields, the acceptance and the efficiency for Λ and $\bar{\Lambda}$ has to be determined. This is done by embedding into real d+Au events simulated Λ decays that were run through a GEANT model of the detector and a simulator of the FTPC response. The reconstruction efficiency for Λ and $\bar{\Lambda}$ in the range $2.5 < |y| < 3.0$ and $0.5 < p_T < 2.0$ GeV/c is ~6% with a small dependence on p_T. This

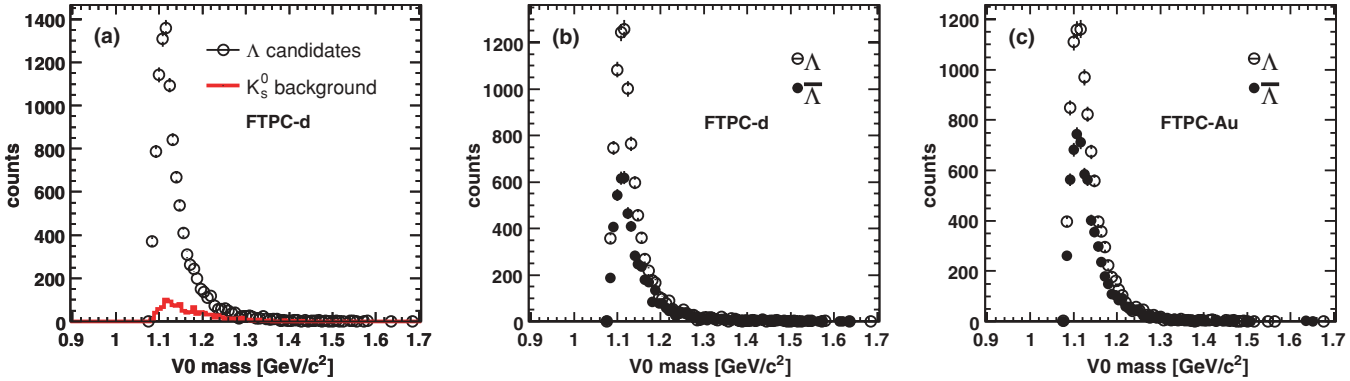

FIG. 1. (Color online) (a) Invariant mass distribution of Λ candidates on the deuteron side with estimated K_s^0 background distribution; (b) and (c) show the background-subtracted Λ and $\bar{\Lambda}$ invariant mass distributions. The widths of the peaks are due to the limited momentum resolution of the detectors and are reproduced by simulations.

number includes the effect of detector acceptance and the analysis cuts used. It is dominated by the requirement of a well-separated decay vertex. The branching ratio of the decay into charged particles is 64%, leading to an overall efficiency of ∼4%.

III. PARTICLE SPECTRA AND YIELDS

Transverse momentum spectra for Λ and $\bar{\Lambda}$ in d+Au minimum bias collisions at $\sqrt{s_{NN}} = 200$ GeV are shown in Fig. 2 for both sides of the collision. An incorrect treatment of defective electronics in FTPC-Au during data production led to the inclusion of noisy electronics channels in the data analysis, affecting the measurements at low p_T in particular. This is due to an excess of low p_T tracks that fulfill the dca cuts for decay daughters, which manifests itself in a shifting of the reconstructed invariant mass at low p_T. Thus the region below $p_T = 0.7$ GeV/c is excluded from the analysis on the Au side. Also shown are fits to the data with a Boltzmann distribution

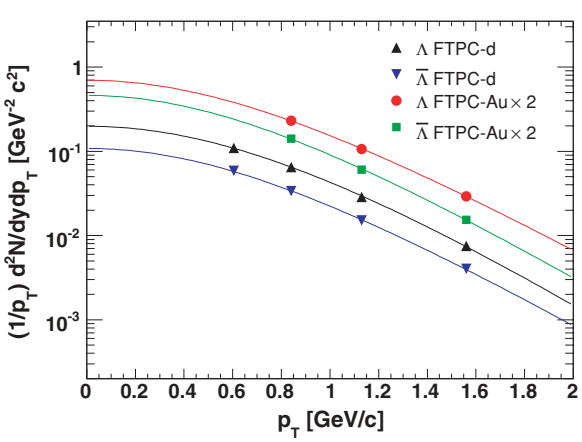

FIG. 2. (Color online) Λ and $\bar{\Lambda}$ spectra on the deuteron and gold sides in d+Au minimum bias collisions. The data points on the gold side are multiplied by 2 for better visibility. The statistical errors are smaller than the points marking the measurements. The curves show a fit with a Boltzmann function in transverse mass to the data points.

in transverse mass m_T, that is,

$$\frac{1}{2\pi p_T}\frac{d^2N}{dy\,dp_T} = Cm_T \exp(-m_T/T), \tag{1}$$

where T is the inverse slope parameter of the spectrum and C is the overall normalization. The spectra on both collision sides agree well with the assumed exponential behavior.

From the fits, the total particle yield in the rapidity range $2.5 < |y| < 3.0$ is extrapolated and the inverse slope parameters are extracted. The missing low p_T measurement in the p_T spectra on the Au side leads to an additional systematic error both in the yield and the inverse slope parameter. The Λ and $\bar{\Lambda}$ yields as well as the inverse slope parameters are determined for minimum bias events and the three individual centrality classes: central (0–20%), midcentral (20–40%), and peripheral (40–100%) events. The particle yields are corrected for acceptance, efficiency, and feed-down from weak decays of hyperons with higher mass. The feed-down contribution is taken from HIJING simulations. The fraction of detected Λ and $\bar{\Lambda}$ particles originating from decays of higher mass hyperons was determined to be 0.1 ± 0.03. This number includes the differences in reconstruction efficiencies for primary $\Lambda(\bar{\Lambda})$ and for $\Lambda(\bar{\Lambda})$ from hyperon decays due to their displaced production point. As usual in heavy-ion collisions, no correction is applied for the contribution from Σ^0 decays. Thus all quoted Λ yields consist of the contributions of primary Λ and Σ^0. Table II summarizes the particle yields, while Table III shows the inverse slope parameters determined from the Boltzmann fits to the spectra as well as the $\bar{\Lambda}/\Lambda$ yield ratio determined from the particle yields. Within the assumption of a Boltzmann distribution, the observed slope parameters translate into mean transverse momenta $\langle p_T \rangle$ between 0.74 and 0.82 GeV/c. Within that assumption, the fraction of the total yield that is covered by the measurement is ∼64% on the d side and ∼43% on the Au side.

The systematic errors quoted for the results include several contributions. These contributions are the cut parameters, the efficiency determination from embedding, background normalization, and feed-down corrections. The size of each contribution is obtained from the size of effects on the results from variations of cuts and normalizations and from

TABLE II. Corrected yields of Λ, $\bar{\Lambda}$, and net Λ on both sides of the collision. In addition to the quoted systematic errors there is an overall normalization uncertainty of 10% on the particle yields.

Centrality	$\Lambda dN/dy$	$\bar{\Lambda} dN/dy$	Net $\Lambda dN/dy$
		Deuteron side ($y = 2.75$)	
Min. bias	$0.067 \pm 0.001(\text{stat})^{+0.010}_{-0.009}(\text{syst})$	$0.035 \pm 0.001(\text{stat})^{+0.006}_{-0.005}(\text{syst})$	$0.032 \pm 0.002(\text{stat}) \pm 0.004(\text{syst})$
top 20%	$0.106 \pm 0.003(\text{stat})^{+0.016}_{-0.014}(\text{syst})$	$0.054 \pm 0.002(\text{stat})^{+0.010}_{-0.008}(\text{syst})$	$0.052 \pm 0.004(\text{stat}) \pm 0.007(\text{syst})$
20–40%	$0.094 \pm 0.003(\text{stat})^{+0.014}_{-0.013}(\text{syst})$	$0.047 \pm 0.002(\text{stat})^{+0.009}_{-0.007}(\text{syst})$	$0.047 \pm 0.004(\text{stat}) \pm 0.006(\text{syst})$
40–100%	$0.045 \pm 0.001(\text{stat})^{+0.007}_{-0.006}(\text{syst})$	$0.025 \pm 0.001(\text{stat}) \pm 0.004(\text{syst})$	$0.020 \pm 0.002(\text{stat}) \pm 0.003(\text{syst})$
		Gold side ($y = -2.75$)	
Min. bias	$0.118 \pm 0.004(\text{stat})^{+0.030}_{-0.028}(\text{syst})$	$0.072 \pm 0.002(\text{stat}) \pm 0.022(\text{syst})$	$0.046 \pm 0.004(\text{stat}) \pm 0.006(\text{syst})$
top 20%	$0.294 \pm 0.017(\text{stat})^{+0.074}_{-0.070}(\text{syst})$	$0.176 \pm 0.010(\text{stat}) \pm 0.054(\text{syst})$	$0.118 \pm 0.020(\text{stat}) \pm 0.015(\text{syst})$
20–40%	$0.163 \pm 0.008(\text{stat})^{+0.041}_{-0.039}(\text{syst})$	$0.096 \pm 0.005(\text{stat}) \pm 0.029(\text{syst})$	$0.067 \pm 0.009(\text{stat}) \pm 0.009(\text{syst})$
40–100%	$0.048 \pm 0.002(\text{stat}) \pm 0.012(\text{syst})$	$0.031 \pm 0.002(\text{stat}) \pm 0.009(\text{syst})$	$0.017 \pm 0.003(\text{stat}) \pm 0.003(\text{syst})$

a comparison of measurements in different subregions of the detectors. The dominating contributions are from uncertainties introduced by the cut selection and from the efficiency determination. This contribution is up to 12% on the deuteron side and as large as 20% on the Au side. Since both the background and feed-down contributions in the raw signal are relatively small, the large uncertainties on their normalizations do not lead to sizable systematics on the extracted yields. Systematics are evaluated separately for the particle yields and the $\bar{\Lambda}/\Lambda$ ratio. In the determination of the net Λ yield and of the $\bar{\Lambda}/\Lambda$ ratio, a significant fraction of the systematic effects cancel, leading to smaller overall systematics in these quantities compared to the Λ and $\bar{\Lambda}$ yields. Especially in the case of the yields, the systematics on the Au side are considerably larger than on the d side due to the aforementioned problems with the treatment of noisy electronics channels.

As an additional systematic check, the fits to the spectra were also performed with an exponential function in m_T of the form

$$\frac{1}{2\pi p_T}\frac{d^2N}{dy\,dp_T} = C' \exp(-m_T/T'), \tag{2}$$

where T' is the inverse slope parameter of the exponential function and C' is the overall normalization. The yields extracted with this exponential function are consistent with the yields extracted based on the assumption of a Boltzmann distribution. Our systematic errors do not include yield variations due to different spectrum functions.

In addition to the systematic errors associated with the analysis, there is a 10% overall normalization uncertainty in the particle yields [18]. This uncertainty is included in the systematic errors shown in the model comparison figures and in the baryon transport study.

To investigate the mechanisms that drive particle production at forward and backward rapidity in d+Au collisions, the measured minimum bias yields are compared with a variety of model calculations. Figure 3 shows the measured $\bar{\Lambda}$ and net Λ yield compared with model calculations. While the $\bar{\Lambda}$ yield is sensitive to the amount of Λ-$\bar{\Lambda}$ pair production, the net Λ yield is strongly influenced by baryon number transport in the collision. Incoming nucleons can be transformed to Λ via the associated production of strangeness, $N + N \rightarrow N + \Lambda + K$, leading to a strong correlation of net Λ and net baryon numbers.

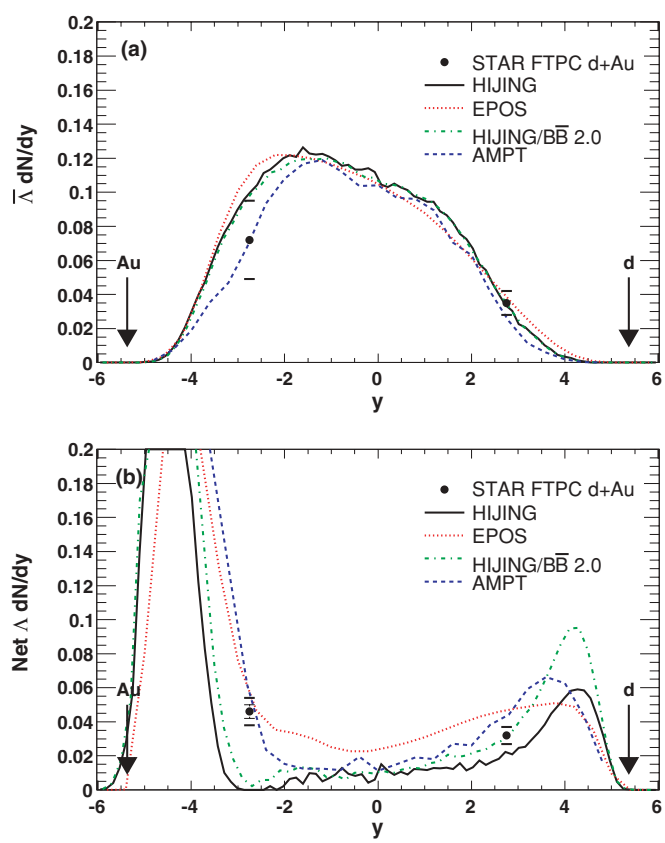

FIG. 3. (Color online) Comparisons of (a) measured $\bar{\Lambda}$ yield with model calculations and (b) net Λ yield with model calculations. Statistical errors are shown as vertical error bars, the vertical caps show the quadratic sum of statistical and systematic errors including the overall normalization uncertainty. Target and projectile beam rapidities are indicated by arrows.

The four models used are based on different principles. HIJING [13] treats nucleus-nucleus collisions as a superposition of individual nucleon-nucleon collisions with a parametrization of nuclear effects such as shadowing and does not include final state effects such as scattering in the hadronic phase. The HIJING/B$\bar{\text{B}}$ model [14,15] is based on HIJING but includes baryon junction interactions for increased baryon number transport. These gluonic structures facilitate baryon number transfer over large rapidity intervals [23]. AMPT [10,11] is a multiphase model that includes a HIJING-like treatment of initial nucleon-nucleon reactions as well as a later rescattering phase. EPOS [12] is a phenomenological approach based on a parton model. It incorporates nuclear effects via parton ladders and target and projectile remnants. None of the model calculations have been tuned to provide agreement with the data presented here, except in the case of HIJING/B$\bar{\text{B}}$. Here the version with a string tension constant of $\kappa_i = 1.5$ GeV/fm is used, since this showed the best agreement with the $\bar{\Lambda}$ yields on both the d and the Au side and thus with the observed Λ-$\bar{\Lambda}$ pair production. For all model comparisons discussed below, the systematic errors in the model calculations are not considered.

On the deuteron side, the HIJING description of several consecutive nucleon-nucleon reactions that take place as the nucleons of the deuteron pass through the gold nucleus is assumed to be appropriate. It is expected that all models should give good descriptions of particle production on the deuteron side. On the gold side, however, effects associated with final state rescattering and the breakup of the target nucleus are expected to play a major role, so the AMPT and EPOS models are expected to show a better performance.

Comparing the $\bar{\Lambda}$ measurements with the rapidity distributions predicted by the models, shown in Fig. 3(a), it is apparent that indeed the deuteron side is very well described, with all models yielding the same result. On the gold side, AMPT is below the other three models. It agrees best with the data; however, also the two HIJING models and EPOS are consistent with the measurement. In general, all models used give a fair description of the $\bar{\Lambda}$ yield and thus of the Λ-$\bar{\Lambda}$ pair production in minimum bias d+Au collisions.

Larger differences are seen for the net Λ yield shown in Fig. 3(b), which is very sensitive to baryon transport, since the Λ has two quarks in common with a nucleon and thus can easily be produced from a nucleon via associated production of strangeness. On the deuteron side, HIJING/B$\bar{\text{B}}$ shows the best agreement with the data, suggesting multiple nucleon-nucleon collisions with additional baryon transport are an appropriate description of the deuteron side of the collision. On the gold side, significant differences between the models are apparent. Neither HIJING nor HIJING/B$\bar{\text{B}}$ reproduce the measured net Λ yield at negative rapidity, while AMPT and EPOS do. This suggests that target-related effects, as implemented in AMPT and EPOS, have a strong influence on strangeness production on the Au side. It appears that at least either a final state rescattering phase, as implemented in AMPT, or the inclusion of target remnants in EPOS is necessary to reproduce the observed net Λ yield on the gold side of the reaction.

Figure 4 shows the $\bar{\Lambda}$ and net Λ yields for the three separate centrality bins compared with calculations with HIJING, HIJING/B$\bar{\text{B}}$ (net Λ only), AMPT, and EPOS. The agreement of the models with the $\bar{\Lambda}$ yields on the deuteron side observed for the minimum bias data set holds for centrality selected collisions. The evolution of the $\bar{\Lambda}$ yield as a function of centrality on the Au side exceeds the increase predicted by the HIJING model. While the $\bar{\Lambda}$ yield in peripheral events agrees best with the AMPT prediction, the central result is consistent with all three models. In general, the yield increase on the gold side significantly exceeds the yield increase on the deuteron side with increasing collision centrality. The behavior of the net Λ yield as a function of centrality is consistent with the observations in minimum bias collisions. While HIJING/B$\bar{\text{B}}$ provides the best match to the data on the deuteron side, the

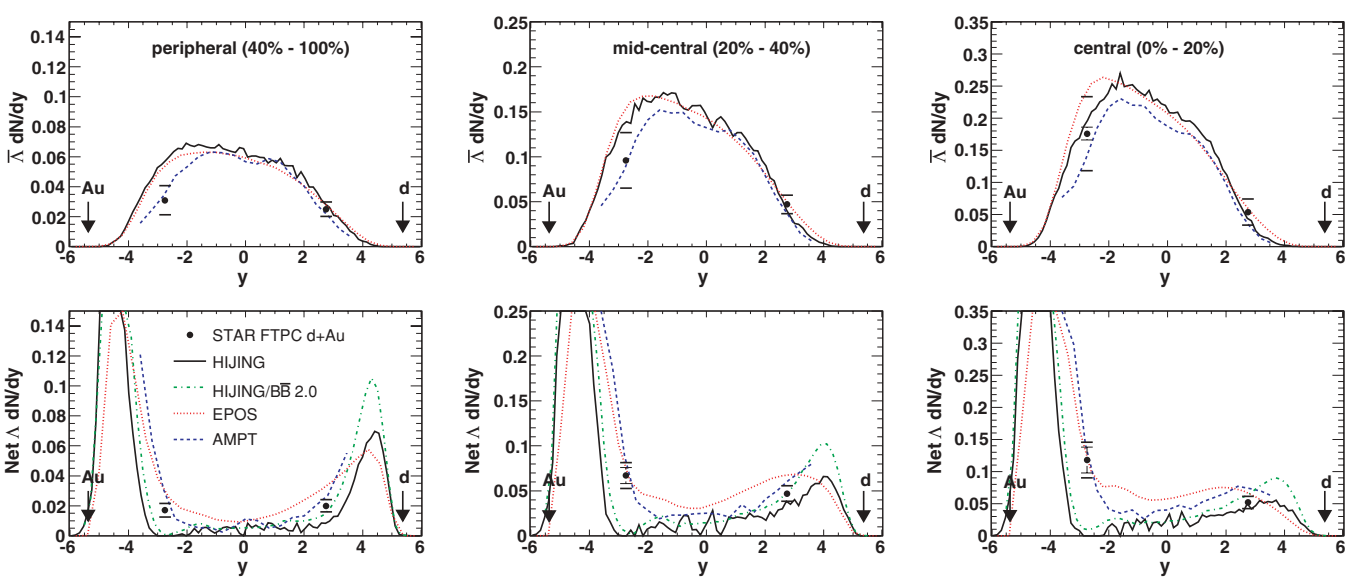

FIG. 4. (Color online) Comparison of $\bar{\Lambda}$ and net Λ yields to model calculations for all three centrality classes. Statistical errors are shown as vertical error bars, the vertical caps show the quadratic sum of statistical and systematic errors. Beam rapidity is indicated by arrows.

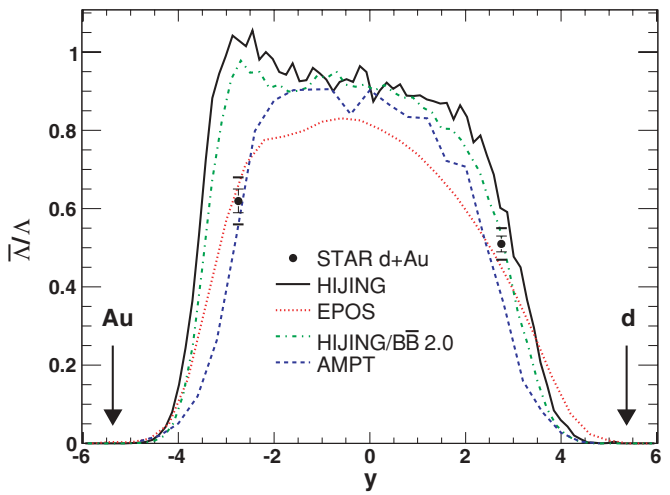

FIG. 5. (Color online) Minimum bias $\bar{\Lambda}/\Lambda$ ratio compared with model calculations. On the deuteron side HIJING/B$\bar{B}$ shows the best agreement with the results, while on the Au side only AMPT and EPOS give a satisfactory description of the data.

gold side is not described by the HIJING models. EPOS and AMPT are able to describe the centrality evolution of the net Λ yield on the Au side. On the deuteron side, all models indicate a transition from large transparency to significant stopping in the probed centrality range. This behavior will be further investigated in Sec. IV.

The minimum bias $\bar{\Lambda}/\Lambda$ yield ratio together with predictions from the four models discussed above is shown in Fig. 5. As for the net Λ yields, all models are close to the data on the deuteron side with HIJING/B$\bar{B}$ showing the best match. On the gold side, AMPT and EPOS, which both incorporate nuclear effects, can reproduce the measurement.

An interesting feature of the centrality dependence of the $\bar{\Lambda}/\Lambda$ ratio, shown in the upper panels of Fig. 6, is that while the measured net Λ yields change significantly with centrality on both sides of the collision in the measured rapidity bins, the ratio stays constant within statistical errors. This shows that the increase in baryon stopping with collision centrality is not reflected in a decrease of the antibaryon to baryon ratio, at least not in the hyperon sector. While the net Λ yield, given by the difference of the Λ and $\bar{\Lambda}$ yields, is directly linked to the amount of baryon number transport in the reaction, the antiparticle to particle ratio is influenced by baryon transport and $\bar{\Lambda}$-Λ pair production. The centrality independence of the ratio suggests that baryon number transport and pair production increase in a similar way with increasing collision centrality and thus with the amount of nuclear material traversed by the projectile. This is shown in the lower panel of Fig. 6 with the net Λ and the $\bar{\Lambda}$ yield as a function of centrality on both collision sides. This is in line with previous $p + A$ measurements with a proton beam of up to 300 GeV on a fixed target which showed very similar $\bar{\Lambda}/\Lambda$ ratios for p+Be and p+Pb reactions [24]. These measurements were performed on the projectile (p) side of the collision as a function of x_F, defined as $p_{||,\Lambda}/p_{\max}$, where $p_{||,\Lambda}$ is the longitudinal component of the Λ momentum and $p_{\max}$ is the maximal possible longitudinal momentum of the Λ in the center-of-mass frame (of a nucleon-nucleon system). The x_F range of these measurements was ~0.2 to ~0.4, compared with an x_F of ~0.1 for the d side data presented here.

From the inverse slope parameters listed in Table III, it can be seen that the inverse slopes of both Λ and $\bar{\Lambda}$ show a collision side dependent behavior with centrality. Within statistical errors, the inverse slope parameter does not change with the number of collisions on the gold side. On the deuteron side, an increase with centrality and thus with the number of nucleon-nucleon collisions the deuteron constituents participate in is

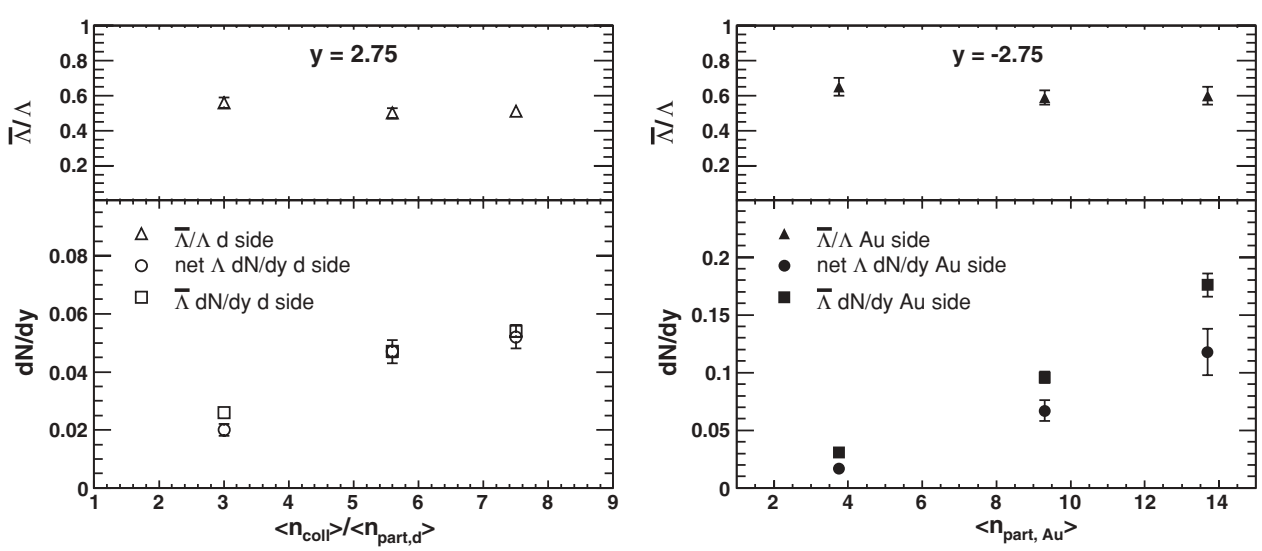

FIG. 6. $\bar{\Lambda}/\Lambda$ ratio and net Λ and $\bar{\Lambda}$ yields as functions of collision centrality on both the deuteron (left) and the gold side (right). On the deuteron side, centrality is expressed by the number of collisions per deuteron participant, while on the gold side the number of Au participants is chosen. Only statistical errors are shown. The increase in baryon number transport with centrality, shown by the net Λ yield, is matched by the increase of $\bar{\Lambda}$-Λ pair production, thus keeping the $\bar{\Lambda}/\Lambda$ ratio constant over a wide centrality range.

TABLE III. Inverse slope parameters determined from Boltzmann fit in m_T for Λ and $\bar{\Lambda}$ on both sides of the collision and $\bar{\Lambda}/\Lambda$ yield ratios.

Centrality	Λ inverse slope (GeV)	$\bar{\Lambda}$ inverse slope (GeV)	$\bar{\Lambda}/\Lambda$ yield ratio
		Deuteron side ($y = 2.75$)	
Min. bias	0.209 ± 0.003(stat) ± 0.009(syst)	0.210 ± 0.004(stat) ± 0.009(syst)	0.52 ± 0.02(stat) ± 0.04(syst)
Top 20%	0.221 ± 0.005(stat) ± 0.010(syst)	0.224 ± 0.007(stat) ± 0.010(syst)	0.51 ± 0.02(stat) ± 0.05(syst)
20–40%	0.208 ± 0.005(stat) ± 0.010(syst)	0.213 ± 0.007(stat) ± 0.010(syst)	0.50 ± 0.03(stat) ± 0.05(syst)
40–100%	0.202 ± 0.004(stat) ± 0.009(syst)	0.199 ± 0.005(stat) ± 0.009(syst)	0.56 ± 0.03(stat) ± 0.05(syst)
		Gold side ($y = -2.75$)	
Min. bias	0.219 ± 0.005(stat) ± 0.013(syst)	0.206 ± 0.005(stat) ± 0.012(syst)	0.61 ± 0.03(stat) ± 0.05(syst)
Top 20%	0.217 ± 0.006(stat) ± 0.013(syst)	0.210 ± 0.007(stat) ± 0.012(syst)	0.60 ± 0.05(stat) ± 0.05(syst)
20–40%	0.218 ± 0.007(stat) ± 0.013(syst)	0.204 ± 0.008(stat) ± 0.012(syst)	0.59 ± 0.04(stat) ± 0.05(syst)
40–100%	0.221 ± 0.007(stat) ± 0.013(syst)	0.201 ± 0.008(stat) ± 0.011(syst)	0.65 ± 0.05(stat) ± 0.05(syst)

observed. This effect is attributed to an increase of the mean transverse momentum of the particles in each of the subsequent collisions the deuteron participants suffer on their way through the gold nucleus, and agrees with the picture of the deuteron side of the reaction discussed above. This observation is in contrast to the behavior of inclusive charged hadrons in d+Au collisions where an increase of the mean p_T with centrality was observed on the Au side, while no centrality dependence was found on the deuteron side [25]. This suggests a difference in the behavior of hyperons and charged hadrons, mainly pions, in the dynamical evolution of the nuclear collision.

From the Λ and $\bar{\Lambda}$ spectra and yields at forward and backward rapidities in d+Au collisions, it is indicated that the deuteron side of the collision is dominated by multiple consecutive nucleon-nucleon collisions of participants of the incoming deuteron with gold nucleons. On the gold side, the HIJING models cannot reproduce the observed net Λ production, while models including nuclear effects can. This situation is different from that found for inclusive charged hadron yields in d+Au collisions at midrapidity and forward rapidity, where no significant sensitivity to various model calculations has been observed [25]. Studies at midrapidity suggest that more differential measurements, such as the ratio of particle production at backward rapidity to forward rapidity as a function of p_T, can provide additional information on the relative contributions of various physical processes to particle production [26,27]. Although such a study is beyond the scope of the present work, there is a consistent picture emerging regarding the model preference of the d+Au data at both midrapidity and forward rapidity. Specifically, midrapidity studies do not support models based on incoherent initial multiple partonic scattering and independent fragmentation, such as HIJING. The EPOS model, which provides a good match to the measurements on Λ production presented here was also found to explain the data at midrapidity in d+Au collisions across many observables [26,28].

IV. BARYON TRANSPORT AND NUCLEAR STOPPING POWER

The discussions in the previous section can be extended to a study of baryon transport in d+Au collisions based on comparisons with the multichain model (MCM) [16]. This model predicts the baryon number transport in nuclear collisions based on simple assumptions. To do this, the net Λ yields presented here have to be related to the total number of net baryons in the corresponding rapidity ranges. This is done using model calculations performed with HIJING/B$\bar{\text{B}}$ [29]. On the Au side of the collision, there are clearly some issues with the description of the net Λ yield by the HIJING/B$\bar{\text{B}}$ model, as discussed above. Thus only the deuteron side in the rapidity range from 0 to 4.0 is used to extract the following correspondence: net baryons $= (10 \pm 1)\times$ net Λ. For the purpose of this discussion, this is assumed to be valid also on the Au side of the reaction. Since the MCM predicts net baryon yields, the model output is scaled by this parameter before comparing it against the data presented here. The model curves are obtained by coupling the MCM as described in Ref. [16] with probability distributions for the number of binary N+N collisions obtained from Glauber calculations.

In the literature, nuclear stopping power is usually described by the mean rapidity loss of incoming baryons in the nuclear collisions [4],

$$\delta y = y_{\text{beam}} - \langle y \rangle, \tag{3}$$

where y_{beam} is the beam rapidity and $\langle y \rangle$ is the mean rapidity of the projectile baryons after the collision. In the MCM, the mean rapidity loss is related to the single phenomenological parameter α by

$$\delta y = (n_{\text{coll}} - 1)/\alpha + 1, \tag{4}$$

where n_{coll} is the number of collisions the incoming nucleon suffers. The distribution of the number of collisions and the probabilities for one or two nucleons of the projectile participating in the reaction are determined with Glauber calculations using the multiplicity based centrality definitions used in the data analysis. The parameter α was originally extracted from an analysis of results on $p + A \rightarrow p + X$ at 100 GeV fixed-target beam energy [30], with a result of $\alpha = 3 \pm 1$.

Figure 7 shows the measured net Λ yields on both sides of the collision for all three centrality bins together with predictions based on the MCM using $\alpha = 2.9$. Uncertainties of the overall scale of the model curves due to the conversion from net baryons to net Λ are on the order of 10% and are

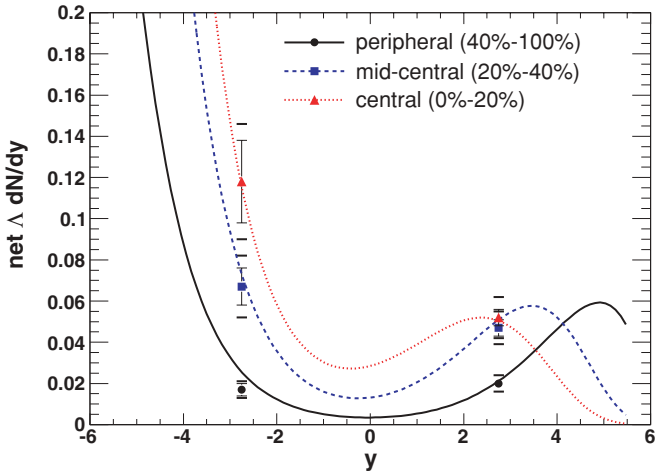

FIG. 7. (Color online) Net $\Lambda dN/dy$ for central, midcentral, and peripheral events on both the deuteron and the Au side of the collision. The data are compared with calculations of the distribution of net baryons obtained with the multichain model [16] with $\alpha = 2.9$, scaled by 0.1 to account for the conversion from net baryons to net Λ. An overall scale uncertainty of 10% on the model curves from this conversion is not shown. See text for details.

not shown here. The value of $\alpha = 2.9$ adopted for the figure is the best fit to the results. Good fits are provided in the range of $\alpha = 2.9 \pm 0.5$, ignoring uncertainties stemming from the conversion from net baryons to net Λ. The data show good agreement with the MCM independent of collision centrality. The range for the model parameter α supported by the data is driven mostly by the measurements on the deuteron side. On the gold side, the net baryon yield is dominated by baryons transported from the target rapidity. The rapidity distribution of baryons on the Au side is only weakly dependent on α, since most participating target (gold) nucleons only suffer one single collision in the reaction, and thus only baryons transported from the projectile side to the target side contribute to an α dependence. The model parameter extracted from the net Λ data in d+Au collisions at $\sqrt{s_{NN}} = 200$ GeV is consistent with that obtained from $p + A$ collisions at 100 GeV fixed target energy.

The good agreement of the MCM with a common parameter for reactions with more than an order of magnitude different center-of-mass energy suggests that the rapidity loss of the incoming baryons in $p(d)$+A collisions and thus the nuclear stopping power is largely independent of beam energy and to a good approximation only a function of the number of collisions over a wide energy range.

In central Au+Au collisions at $\sqrt{s_{NN}} = 200$ GeV, a saturation of the stopping power with energy has been observed that was not seen in previous measurements at lower energy [8]. From the expectations of MCM with $\alpha = 2.9$, it appears that the rapidity loss in central nucleus-nucleus collisions is lower than that in d+Au collisions for a comparable number of collisions per incoming baryon. An important difference between the collisions of large, equal-sized nuclei and collisions of a very small nucleus with a large nucleus is that in the latter case the nucleons of the small nucleus collide with nucleons from the large nucleus that in almost all cases have not participated in the reaction before. This is not true in the first case, which is characterized by multiple collisions of both projectile and target nucleons. This difference can lead to differences in the stopping behavior in the reaction and could lead to the different observations in the two collision systems.

V. CONCLUSION

We have presented measurements of Λ hyperon production in d+Au collisions at $\sqrt{s_{NN}} = 200$ GeV at forward ($y = 2.75$) and backward ($y = -2.75$) rapidity. The comparison of minimum bias yields of $\bar{\Lambda}$ and net Λ to a variety of model calculations shows that the deuteron side is well described by all models used. On the gold side, only AMPT and EPOS are able to explain the net Λ results, suggesting nuclear effects have an influence on hyperon production on the gold side of the collision. The observed centrality independence of the $\bar{\Lambda}$ /Λ ratio shows that baryon number transport through associated production of strangeness and $\bar{\Lambda}$-Λ pair production both have a similar dependence on the number of participants and the number of binary collisions in the reaction. The good agreement of the multichain model with the measured net Λ yields using the same parameter as for lower energy data suggests energy independence of the nuclear stopping power for $p(d) + A$ collisions over a wide range in center-of-mass energy.

ACKNOWLEDGMENTS

We thank L. W. Chen, C. M. Ko, V. Topor-Pop, and K. Werner for providing us the results for the different model calculations and M. Gyulassy for help regarding the multichain model. We thank the RHIC Operations Group and RCF at BNL, and the NERSC Center at LBNL for their support. This work was supported in part by the Offices of NP and HEP within the US DOE Office of Science; US NSF; BMBF of Germany; CNRS/IN2P3, RA, RPL, and EMN of France; EPSRC of the United Kingdom; FAPESP of Brazil; Russian Ministry of Science and Technology; Ministry of Education and the NNSFC of China; IRP and GA of the Czech Republic; FOM of the Netherlands; DAE, DST, and CSIR of the Government of India; Swiss NSF; Polish State Committee for Scientific Research; SRDA of Slovakia; and Korea Science and Engineering Foundation.

[1] J. Adams *et al.* (STAR Collaboration), Nucl. Phys. **A757**, 102 (2005).
[2] C. Adler *et al.* (STAR Collaboration), Phys. Rev. Lett. **89**, 092301 (2002).
[3] K. Adcox *et al.* (PHENIX Collaboration), Phys. Rev. Lett. **89**, 092302 (2002).
[4] W. Busza and A. S. Goldhaber, Phys. Lett. **B139**, 235 (1984).
[5] J. D. Bjorken, Phys. Rev. D **27**, 140 (1983).

[6] T. Alber *et al*. (NA35 Collaboration), Eur. Phys. J. C **2**, 643 (1998).
[7] I. Vitev, Phys. Rev. C **75**, 064906 (2007).
[8] I. Bearden *et al*. (BRAHMS Collaboration), Phys. Rev. Lett. **93**, 102301 (2004).
[9] H. Appelshäuser *et al*. (NA49), Phys. Rev. Lett. **82**, 2471 (1999).
[10] B. Zhang, C. M. Ko, B. A. Li, and Z. W. Lin, Phys. Rev. C **61**, 067901 (2000).
[11] Z. W. Lin and C. M. Ko, Phys. Rev. C **68**, 054904 (2003).
[12] K. Werner, F.-M. Liu, and T. Pierog, Phys. Rev. C **74**, 044902 (2006).
[13] X.-N. Wang and M. Gyulassy, Phys. Rev. D **44**, 3501 (1991).
[14] S. E. Vance and M. Gyulassy, Phys. Rev. Lett. **83**, 1735 (1999).
[15] V. Topor Pop, M. Gyulassy, J. Barrette, and C. Gale, Phys. Rev. C **72**, 054901 (2005).
[16] S. Date, M. Gyulassy, and H. Sumiyoshi, Phys. Rev. D **32**, 619 (1985).
[17] K. H. Ackermann *et al*. (STAR Collaboration), Nucl. Instrum. Methods A **499**, 624 (2003).
[18] J. Adams *et al*. (STAR Collaboration), Phys. Rev. Lett. **91**, 072304 (2003).
[19] K. H. Ackermann *et al*., Nucl. Instrum. Methods A **499**, 713 (2003).
[20] M. Anderson *et al*., Nucl. Instrum. Methods A **499**, 659 (2003).
[21] D. Kharzeev, E. Levin, and M. Nardi, Nucl. Phys. **A730**, 448 (2004).
[22] M. L. Miller, K. Reygers, S. J. Sanders, and P. Steinberg, Annu. Rev. Nucl. Part. Sci. **57**, 205 (2007).
[23] D. Kharzeev, Phys. Lett. **B378**, 238 (1996).
[24] P. Skubic *et al*., Phys. Rev. D **18**, 3115 (1978).
[25] B. I. Abelev *et al*. (STAR Collaboration), Phys. Rev. C **76**, 054903 (2007).
[26] B. I. Abelev *et al*. (STAR Collaboration), nucl-ex/0609021.
[27] J. Adams *et al*. (STAR Collaboration), Phys. Rev. C **70**, 064907 (2004).
[28] J. Adams *et al*. (STAR Collaboration), Phys. Lett. **B637**, 161 (2006).
[29] V. Topor-Pop (private communication).
[30] D. S. Barton *et al*., Phys. Rev. D **27**, 2580 (1983).